Unified calculation of generalized oscillator strength of argon ranging from bound to continuum states

Xiang Gao,[1,2,*] Rui Jin,[1,2] De-Ling Zeng,[1,3] Xiao-Ying Han,[4] Jun Yan,[4] and Jia-Ming Li[2,3,5]

[1]*Beijing Computational Science Research Center, Beijing 100094, China*

[2]*Department of Physics and Center for Atomic and Molecular Nanosciences, Tsinghua University, Beijing 100084, China*

[3]*Key Laboratory for Laser Plasmas (Ministry of Education) and Department of Physics and Astronomy, Shanghai Jiao Tong University, Shanghai 200240, China*

[4]*Institute of Applied Physics and Computational Mathematics, Beijing 100088, China*

[5]*Collaborative Innovation Center of Quantum Matter, Beijing 100084, China*

(Received 23 June 2015; published 25 November 2015)

The electron and photon scattering data of an atom are crucial for many scientific fields, including plasma physics, astrophysics, and so on. For high enough but nonrelativistic incident energies, the first Born approximation is applicable for calculating these data, in which the key physics quantity is the generalized oscillator strength (GOS). In high-energy electron impact excitation processes, atoms will be excited into various excited states including strongly perturbed Rydberg and adjacent continuum states. How to calculate these quantities of a nontrivial many-electron atom rapidly and accurately is still a great challenge. Based on our eigenchannel R-matrix method R-eigen, we further extend it to calculate the GOS of a whole channel in an atom, which includes all Rydberg and adjacent continuum states. The $J^{\pi} = 1^{-}$ states of argon are chosen as an illustrating example. The calculation results are in good agreement with the available benchmark absolute experimental measurements. The calculated eigenchannel GOS matrix elements are smooth functions of the excitation energy and momentum transfer. From such smooth eigenchannel GOS matrix elements, we can obtain the GOS of any specific excited state through multichannel quantum defect theory, e.g., infinite Rydberg (including a strongly perturbed one), autoionization, and continuum states.

DOI: 10.1103/PhysRevA.92.052712 PACS number(s): 34.80.Dp, 31.15.−p, 32.70.Cs, 34.50.Fa

I. INRODUCTION

The electron and photon scattering data of an atom are crucial for many scientific fields, including plasma physics, astrophysics, and so on [1]. For high enough but nonrelativistic incident energies, the first Born approximation is applicable [2,3] for calculating these data, in which the key physics quantity is the generalized oscillator strength (GOS). The GOS (also called the form factor in other fields such as nuclear and particle physics) describes quantitatively the inelastic scattering processes of a fast electron (photon) within the first Born approximation (FBA), where the differential scattering cross section is proportional to the GOS. The GOS is a function of the momentum transfer K and energy transfer ΔE of the target. In the limit of zero momentum transfer, the GOS becomes equal to the optical oscillator strength (OOS) [2]. This connects the high-energy electron impact excitation process with the photoabsorption or photoionization processes. Therefore GOS offers unique information about the nature of the electronic transitions and the electron scattering process of atoms and molecules. It is also a basic ingredient for the study of intercombination transitions in collisions of electrons with Rydberg atoms [4] and for the calculation of a collision of a Rydberg atom with a neutral atom in the free electron model [5]. It can be used in calculations of the stopping power of electrons, which is the key physical quantity to describe the energy deposition of electrons passing through matter [6] and hence is very necessary for many fields, such as radiology, health physics [7], and so on.

Numerous experimental and theoretical investigations have been carried out over the past 60 years [2,3,8] and both have made great progress. Benchmark absolute experimental measurements have been successfully carried out for valence-shell excitations of noble atoms of He [9], Ne [10], Ar [11,12], and Kr [13] by high-energy electron energy loss spectroscopy (EELS) and by inelastic x-ray scattering (IXS) recently [14,15]. Bethe has calculated the GOS of the hydrogen atom, known as the Bethe surfaces, to exemplify and illustrate the general features of the GOS [16]. From then on, various theoretical methods have been developed, such as the calculation using hydrogen-like wave functions with an effective nuclear charge [17], the independent particle model [18], the random phase approximation with exchange [19], the R-matrix method [20] and so on. However, these investigations are mainly focused on some specific transitions among the low excited states of targets, which cannot satisfy the needs in many related scientific fields. For example, for the calculation of stopping power, the GOS of all kinematically accessible exited states of an atom or molecule, including discrete as well as continuum states are needed [6]. Furthermore, for theoretical studies of non-hydrogen-like atoms, the GOS is very sensitive to the quality of many-electron wave functions, where the convergence is not easy to achieve. Therefore, the appropriate theoretical method to provide enormous reliable GOS data of non-hydrogen-like atoms needs to be developed.

Based on the analytic continuation property of scattering matrices, there exist intimate relations between atomic energy levels and the related electron-ion collision processes [21–24]. In the framework of multichannel quantum defect theory (MQDT) [21–24], with a set of physical parameters (i.e.,

*xgao@csrc.ac.cn

short-range scattering matrices) which vary smoothly with the excitation energy, all the Rydberg states, autoionization states, and adjacent continuum states can be described in a unified manner [21–24]. According to MQDT, the energy eigenstate is a superposition of eigenchannels and the coefficients of the superposition can be calculated analytically by the boundary conditions at infinity. Thus the calculation of the transition matrix elements from a specific initial state to any final state can be reduced to the calculation of the transition matrix elements from a specific initial state to final eigenchannels, which vary smoothly with the final eigenchannel energy. We have developed the eigenchannel R-matrix method (ECR) referred to as R-eigen and R-R-eigen [25], to directly calculate short-range scattering matrices as well as eigenchannel wave functions in the whole energy regions of interest, i.e., either the discrete energy region or the continuum energy region, on equal footing. With our ECR method, the short-range scattering matrices in the discrete energy region can be calculated with enough accuracy which can be determined readily by comparisons with precise spectroscopic measurements [26] based on multichannel quantum defect theory (MQDT) [21–24]. Through the analytical continuation properties of short-range scattering matrices, their accuracy in the whole energy regions can be ascertained [25]. With the corresponding high-quality eigenchannel wave functions, various transition matrix elements can be readily calculated, such as the OOS of the optical transitions. For the optical transition processes, the OOS of infinite-bound-type Rydberg states will connect with the continuum photoionization cross sections through the physical quantities oscillator strengths densities (OOSD), where the OOS and OOSD is linked by density of states (DOS) [27]. It is straightforward to extend this concept to define the generalized oscillator strength densities (GOSD), by which the GOS of infinite Rydberg, autoionization, and continuum states of a nontrivial many-electron atom can be treated in a unified manner.

In the present work, we further develop the eigenchannel R-matrix method to calculate the GOSD of atoms. The multichannel transition matrix elements of GOS of eigenchannels can be calculated and found to be smooth functions of the momentum transfers and the excitation energies. From such smooth eigenchannel GOS matrix elements, we can obtain the GOSD of any specific excited state very quickly through MQDT without missing any one, e.g., infinite Rydberg (including a strongly perturbed one), autoionization, and continuum states (correspond to impact ionization process). Furthermore, the information of short-range dynamical interactions can be unveiled in detail from our treatment, such as the $s-d$ wave mixings due to the quadrupole polarization interaction. As an illustrative example, we will present our recent calculation results of Ar, which are in good agreement with the available absolute benchmark experiments [11,12,15].

II. THEORETICAL METHOD AND CALCULATION RESULTS

For high-energy electron impact excitation processes, atoms will be excited into various excited states, i.e., various strongly perturbed Rydberg and adjacent continuum states. Since there are infinite excited states involved in the high-energy electron collision processes, how to calculate these wave fuctions of a many-electron atom rapidly and accurately is a great challenge. Over the years, the R-matrix approach has been successfully developed as an *ab initio* method for treating a variety of dynamical processes in atomic physics [24,28–30], including the bound states and continuum states. However, the traditional R-matrix method treats each state separately, which is inconvenient to calculate all states together and ascertain the accuracies. From the point of view of MQDT, the N-electron ion core target states and the excited electron with the appropriate angular momentum couplings form channels for the $N+1$-electron excited complex with a specific total angular momentum. The wave functions belonging to the same channel will share some common properties. Recently, we have extended both the nonrelativistic and relativistic versions of the eigenchannel R-matrix (ECR) method, referred to as R-eigen and R-R-eigen, respectively [25], from the earlier Breit-Pauli [28] and Dirac R-matrix codes [29]. With the ECR method, we are able to calculate the short-range scattering matrices corresponding to the physical parameters associated with the multichannel quantum defect theory (MQDT) [21–24] and the related wave functions for both the discrete and continuous energy regions of interest. Various physical quantities can then be derived from a straightforward application of the MQDT procedure.

For excited Ar atoms with $J^\pi = 1^-$, in the energy regions near the first and second ionization thresholds [$\mathrm{Ar}^+(^2P_{3/2})I_{3/2}$ and $\mathrm{Ar}^+(^2P_{1/2})I_{1/2}$], there are $N=5$ physical ionization channels, namely, $\mathrm{Ar}^+(^2P_{3/2})nd_{3/2}/\varepsilon d_{3/2}$, $\mathrm{Ar}^+(^2P_{3/2})nd_{5/2}/\varepsilon d_{5/2}$, $\mathrm{Ar}^+(^2P_{3/2})ns_{1/2}/\varepsilon s_{1/2}$, $\mathrm{Ar}^+(^2P_{1/2})ns_{1/2}/\varepsilon s_{1/2}$, and $\mathrm{Ar}^+(^2P_{1/2})nd_{3/2}/\varepsilon d_{3/2}$, where $nd_{3/2}/\varepsilon d_{3/2}$ represents a bound or continuum $d_{3/2}$ orbital wave function, respectively. Adopting our modified R-eigen code [25], the short-range scattering matrix $\mathbf{S}$ (with the dimension of $N\times N = 5\times 5$) in the energy region of interest can be calculated directly. The physical eigenchannel parameters of MQDT (i.e., five eigen-quantum defects μ_α and a 5×5 orthogonal transformation matrix $U_{i\alpha}$) are related to the $\mathbf{S}$ matrix as

$$S_{ij}^{J^\pi=1^-} = \sum_{\alpha=1}^{N} U_{i\alpha}\ \exp(i2\pi\mu_\alpha)\ U_{\alpha j}. \tag{1}$$

For the orthogonal transformation matrix $U_{i\alpha}$, it can be further expressed in $N\times(N-1)/2 = 10$ independent generalized Euler angles θ_{lm} [22,25]. Our calculated MQDT physical eigenchannel parameters in $J^\pi = 1^-$ symmetry of Ar are shown in Fig. 1. Because of the analytical property of the short-range $\mathbf{S}$ matrix, both μ_α and θ_{lm} vary smoothly with energies E across the ionization thresholds and calculations only for a few energy points are needed, as shown in Fig. 1. Note that, as the energy region varies, the number of physical eigenchannel may change because of the mathematical properties of Coulomb wave functions (i.e., $\varepsilon_l = E - I_i > \varepsilon_l^c = -1/l^2$, with I_i the threshold of the ion core Φ_i and ε_l^c the lowest orbital energy of the l scattering wave [21,25]. The physical states of any Rydberg type $\Phi_i\varepsilon_l$ should be in the energy regions $E = I_i + \varepsilon_l > E^c = I_i + \varepsilon_l^c$. For a specific energy point, only the physical channels with their channel energies that satisfy the above criterion are relevant to the physical states (i.e., energy eigenstates). Since the physical states associated with the negative orbital energy channels are discrete, there exists

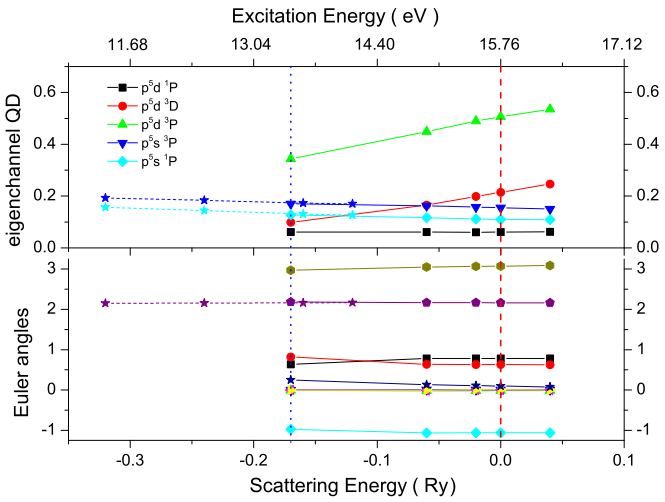

FIG. 1. (Color online) Eigen-quantum defects μ_α, Euler angles θ_k for $U_{i\alpha}$ matrix in $J^\pi = 1^-$ symmetry of Ar. The vertical dotted blue line indicates the connection position of two channels and five channels. The vertical dashed red line is the position of the ionization threshold of $^2P_{3/2}$.

an interval between E_c and E_p (the energy of the first physical state of that channel), where the calculations with two different numbers of physical channels should be identical [25]. The physical parameters of the same eigenchannel in such different channel calculations should interface smoothly. In the case of present $J^\pi = 1^-$ symmetry, the three d-wave physical channels, namely, $Ar^+(^2P_{3/2})nd_{3/2}/\varepsilon d_{3/2}$, $Ar^+(^2P_{3/2})nd_{5/2}/\varepsilon d_{5/2}$, and $Ar^+(^2P_{1/2})nd_{3/2}/\varepsilon d_{3/2}$, cannot exist below the energy $E^c = I_{3/2} + \varepsilon^c_{l=2} = -1/l^2 = -0.25$ Ry ($I_{3/2}$ is zero by our definition). As shown in Fig. 1, the interface energy point we choose for the two-channel and five-channel calculation is around -0.17 Ry, above which the first energy level of the d Rydberg series begins.

The corresponding eigenchannel wave functions [21–24] in the energy region of interest can also be calculated directly using the ECR method. Within the reaction zone (i.e., within the R-matrix box radius), the eigenchannel wave functions can be obtained by solving the $N + 1$-electron problem variationally. Outside the reaction zone, the eigenchannel wave functions with normalization per unit energy can be expressed rigorously as [21–24]

$$\Psi_\alpha = \sum_{i=1}^{N} \Phi_i U_{i\alpha}(f_i \cos\pi\mu_\alpha - g_i \sin\pi\mu_\alpha)\ r \geqslant r_0, \qquad (2)$$

where the index α represents the α th eigenchannel and the indices i are the five ionization channels, f_i and g_i are the regular and irregular Coulomb radial wave functions with normalization per unit energy.

Our eigenchannel calculations have been performed with 30 Ar^+ target states which will form about 100 channels, and 200–300 Ar* bound type configuration state functions (CSFs). Among the 100 channels, there are only five physical channels as mentioned above; more specifically, their radial wave functions at $r = r_0$ are linear combinations of the radial Coulomb wave functions with both positive and negative orbital energies. The rest of the channels and the bound type

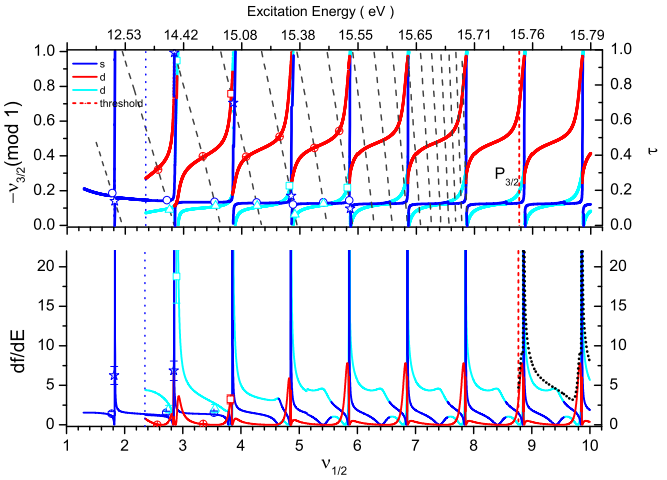

FIG. 2. (Color online) Upper: Quantum defect $-\nu_{3/2}$(mod 1) vs $\nu_{1/2}$ plot of Ar. Various open points are experimental level positions. The solid periodic curves for Eq. (4) and dashed lines for Eq. (5) are shown. The vertical dashed red line indicates the $I_{3/2}$ threshold and the vertical dotted blue line denotes the smooth connection between the two-physical channel calculation and the five-physical channel calculation. Lower: The corresponding oscillator strength densities, where the symbols are consistent with the one in the upper panel.

CSFs are defined as computational channels. They are included in our calculation to assure that the electron correlations are taken into account adequately. With the calculated μ_α and $U_{i\alpha}$, the physical energy-eigen-wave functions are the linear combination of eigenchannel wave functions [21–24]

$$\Psi(E) = \sum_\alpha A_\alpha \psi_\alpha(E), \qquad (3)$$

with the mixing coefficients A_α determined by electron asymptotic boundary conditions based on MQDT [21–24]. For bound states, the asymptotic boundary conditions require [21–24]

$$\sum_{\alpha}^{N=5} U_{i\alpha} \sin\pi(\nu_i + \mu_\alpha) A_\alpha = 0 \quad \text{for all i}, \qquad (4)$$

with the effective principal quantum numbers ν_i defined as

$$E(\text{a.u.}) = I_i + \varepsilon_i = I_i - \frac{1}{2\nu_i^2}, \quad \text{for all i} \qquad (5)$$

Based on Eqs. (4) and (5), all energy levels of a strongly perturbed Rydberg series can be calculated without missing any energy levels. As shown in the upper panel of Fig. 2, the calculated energy levels are represented as the cross points [namely, the roots of Eqs. (4) and (5)] between the periodic solid curves for Eq. (4) and the dashed curves for Eq. (5) [25]. Note that based on the present calculated μ_α only adjusted by a few percent and the calculated $U_{i\alpha}$ without any adjustment, excellent agreements between the calculated energy levels and the precise spectroscopic levels denoted as the open points [26] have been achieved, as shown in the upper panel of Fig. 2.

Above the $I_{3/2}$ threshold, there are three open physical ionization channels, i.e., $Ar^+(^2P_{3/2})\varepsilon d_{3/2}$, $Ar^+(^2P_{3/2})\varepsilon d_{5/2}$, and $Ar^+(^2P_{3/2})\varepsilon s_{1/2}$. Thus, there are three collision eigenphase shifts $\pi \cdot \tau_\rho$ at a fixed $\nu_{1/2}$, which are the three roots of

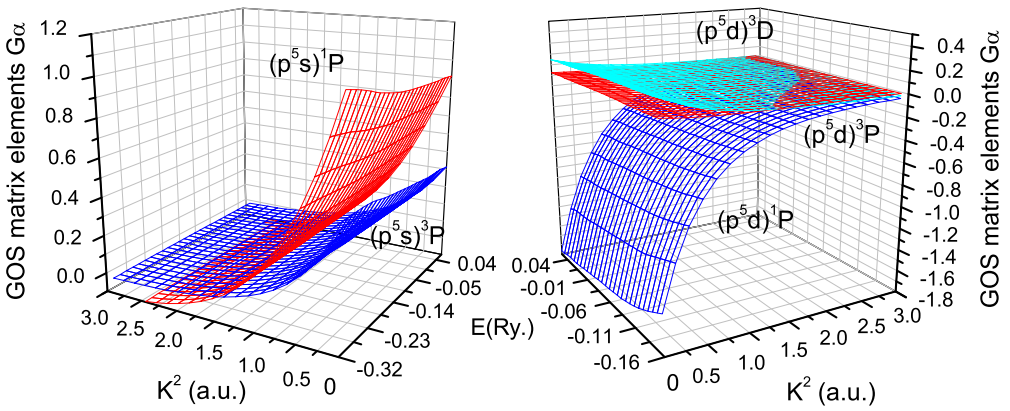

FIG. 3. (Color online) The eigenchannel GOS matrix elements of $J^\pi = 1^-$ symmetry of Ar.

Eq. (4) [22] with the index ρ denotes the three branches. Very interestingly, the three branches τ_ρ smoothly connect with three branches of $-\nu_{3/2}(\mathrm{mod}\,1)$ below the $I_{3/2}$ threshold as shown in the upper panel of Fig. 2. This smooth connection is the consequence of the analytic continuation properties of short-range scattering matrices. Since each energy level belongs to a specific ρ branch, we can clearly see the relations between energy levels and resonant scattering phase shifts in this way. More specifically, the three branches are shown in three different colors in the figure, where the blue one represents the phase shift with s-wave feature, the red and cyan ones represent the phase shifts of two d waves. Below the $I_{3/2}$ threshold, the energy levels form three strongly perturbed Rydberg series denoted as ⊕,◯,△ and two perturbing Rydberg series denoted as ☆,□ respectively, with ◯,☆ having the s-wave character and ⊕,△,□ having the d-wave character. The upper panel of Fig. 2 can also tell us the information of short-range dynamical interactions. For example, the avoid crossings of three eigenphase shifts at the positions of about $\nu_{1/2} = 2.9$, 3.9 illustrate very clearly the strong $s-d$ wave mixings due to the quadrupole polarization interaction. Therefore it should be more physically transparent to characterize the spectroscopic data in the present way. Some more discussions will be presented later in combination with the lower panel of Fig. 2.

With the calculated eigenchannel wave functions $\psi_\alpha(E)$, various physics quantities can be readily calculated, which should also be the smooth function of energy E. Let us focus on the GOS matrix elements. Within the Born approximation, the high-energy electron impact excitation differential cross sections can be written as [20]

$$\frac{d\sigma_n}{d\Omega} = \frac{k'}{k}\left|f_n^B(\hat{k},\hat{k}')\right|^2 = \frac{2}{\Delta E_n}\frac{k'}{k}\frac{F_n(\Delta E_n,K)}{K^2} \tag{6}$$

with the incident high-energy electron momentum $\vec{k}$, the scattered electron momentum $\vec{k}'$, the excitation energy $\Delta E_n = E_n - E_o$, the momentum transfer $\overrightarrow{K} = \overrightarrow{k'} - \vec{k}$. $F_n(\Delta E_n, K)$ is the GOS, which can be expressed as

$$F_n(\Delta E_n,K) = \frac{2\Delta E_n}{K^2}\left|\langle\Psi(E_n)|\sum_{j=1}^{N} e^{i\vec{K}\cdot\vec{r}_j}|\Psi_0\rangle\right|^2. \tag{7}$$

In the limit of zero momentum transfer ($K = 0$), the GOS becomes equal to the OOS. This relation connects the high-energy electron-impact excitation process with the photoabsorption process. The eigenchannel matrix elements of GOS is defined as

$$G_\alpha = <\psi_\alpha|\sum_{j=1}^{N} e^{i\vec{K}\cdot\vec{r}_j}|\Psi_o> /K. \tag{8}$$

Note that when the momentum transfer $K = 0$ for dipole-allowed transitions, G_α is identical to the matrix element of oscillator strength D_α [24]. Figure 3 displays the calculated eigenchannel matrix elements G_α. As shown in Fig. 3, G_α is a smooth function of energy E and momentum transfer K. We can also see that the G_α surfaces of two s waves will intersect with the $G_\alpha = 0$ surface, which in turn will form the nodal structure of the GOS surfaces. For the G_α surfaces of three d waves, it will not intersect with the $G_\alpha = 0$ surface, where no nodal structures will exist. These results are consistent with the laws of the nodal structure obtained from the analysis of the independent particle wave functions [31].

Thus according to Eqs. (3) and (7), the GOS of any energy level E_n of a strongly perturbed Rydberg series can be expressed as

$$F_n(\Delta E_n,K) = \frac{2\Delta E_n}{N_n^2}\left|\sum_\alpha G_\alpha A_{\alpha,n}\right|^2, \tag{9}$$

with the reduced generalized matrix elements G_α defined in Eq. (8), the mixing coefficients $A_{\alpha,n}$ as the solutions of Eq. (4) for the nth energy level corresponding to $(\nu_{3/2,n},\nu_{1/2,n})$ and the normalization factor N_n^2 is defined as Eqs. (2.7) and (2.8) in [22].

For the optical processes, the OOS of infinite bound-type Rydberg states will connect with the continuum photoionization cross sections through the physical quantities OOSD, which is the OOS multiplied by the DOS (i.e., dn/dE) [27]. It is straightforward to extend this concept to the GOS. The GOS F_n of the Rydberg state $(\nu_{1/2,n,\rho},\nu_{3/2,n,\rho})$ will reside in the corresponding GOSD $\frac{dF_n^{(\rho)}}{dE}$, where

$$\frac{\mathrm{dF}_n{}^{(\rho)}(\Delta E,K)}{\mathrm{d}E} = \left(\frac{dn}{dE}\right)_{n,\rho}\cdot F_n^\rho(\Delta E,K) = \frac{2(E-E_0)\left|\sum_\alpha G_\alpha A_{\alpha,n,\rho}\right|^2}{N_{3/2,n,\rho}}. \tag{10}$$

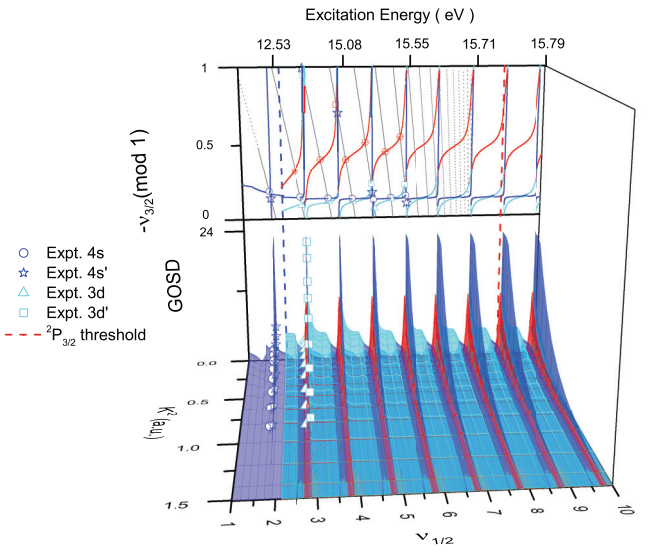

FIG. 4. (Color) The generalized oscillator strength densities of Ar from initial state $3p^6 J^\pi = 0^+$ to final channel $J^\pi = 1^-$.

The expressions for $(\frac{dn}{dE})_{n,\rho}$ and $N_{3/2,n,\rho}$ can be found in Eqs. (5.1) and (2.8) in [22], respectively. Note that as we discussed above, the $\nu_{3/2,n}$ of the nth energy level will connect with a specific branch of autoionization phase shift τ_ρ above the threshold. Therefore we use ρ here to represent this character.

Let us first look at the special case of $K = 0$, which is directly related to the optical processes. The calculated three $\frac{df^{(\rho)}}{dE}$ corresponding to the three ρ branches are shown in three different colors in the lower panel of Fig. 2, with the blue one representing the s wave, the red and cyan ones representing the two d waves. The experimental oscillator strength f_n of the Rydberg state $(\nu_{1/2,n,\rho}, \nu_{3/2,n,\rho})$ [32] will reside in the corresponding oscillator strength density $\frac{df_n^{(\rho)}}{dE}$ as shown in the lower panel of Fig. 2, denoted as ⊕,◯,△, ☆,□. These symbols are consistent with the ones defined in the upper panel of Fig. 2. We can see that the $\frac{df_n^{(\rho)}}{dE}$ also belongs to a specific $\frac{df^{(\rho)}}{dE}$ branch. It is interesting to note that above the $I_{3/2}$ threshold the oscillator strength densities of the overlapping autoionization resonances should be

$$\frac{df}{dE} = \sum_\rho^3 \frac{df^{(\rho)}}{dE} = \sum_\rho^3 \frac{2(E-E_0)\left|\sum_\alpha D_\alpha A_{\alpha,\rho}\right|^2}{N_{3/2,\rho}}, \quad (11)$$

as shown by the dashed line in the lower panel of Fig. 2.

The corresponding three branches of the generalized oscillator strength densities $\frac{dF_{n,\rho}(\Delta E_n, K)}{dE}$ can be readily calculated and shown in Fig. 4. Because of an extra dimension of variable K, the three branches of curves in the lower panel of Fig. 2 will extend to three branches of surfaces, as shown in Fig. 4. Such three surfaces contain all the information of the GOS of all Rydberg states and adjacent continua in the $J^\pi = 1^-$ symmetry.

A few available experimental generalized oscillator strength densities [11,12] are also shown in Fig. 4. For detailed examinations between the calculated and experimental GOS [11,12,15,33–34], Fig. 5 displays comparisons

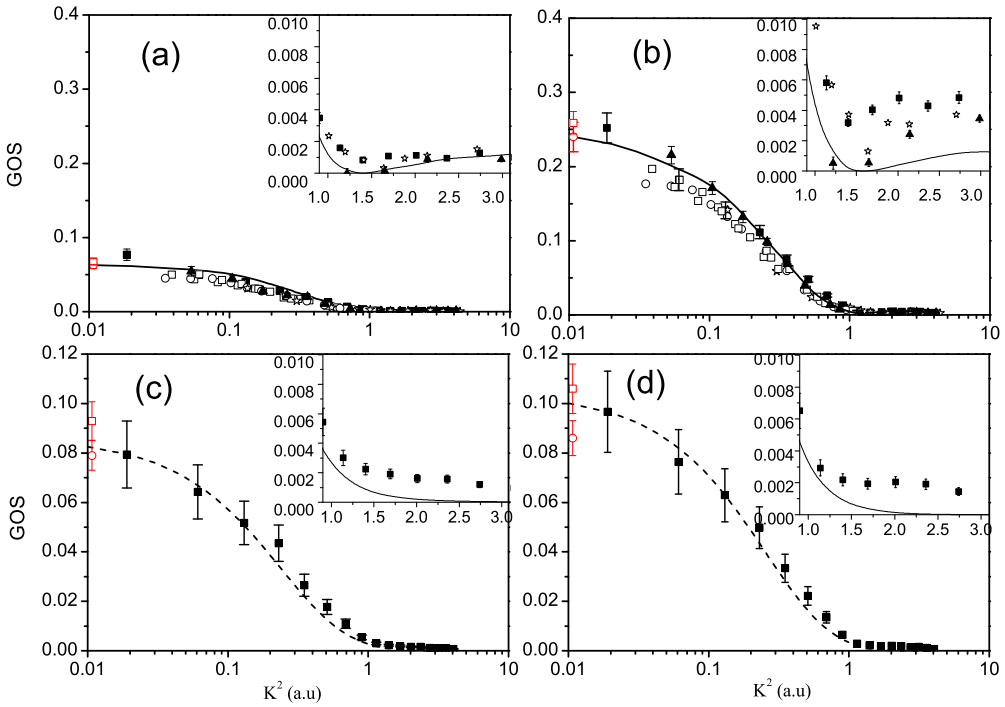

FIG. 5. (Color online) The comparison of the generalized oscillator strength of Rydberg states $3p^5 4s[3/2]_1$, $3p^5 4s'[1/2]_1$, $3p^5 3d[3/2]_1$, and $3p^5 3d'[3/2]_1$ with the experimental measurement.

for the generalized oscillator strength of Rydberg states $3p^5 4s[3/2]_1$, $3p^5 4s'[1/2]_1$, $3p^5 3d[3/2]_1$, and $3p^5 3d'[3/2]_1$. As shown in Fig. 5, our calculated GOS of these low excited states are in good agreement with the recent experimental measurements [11,12,15]. At $K = 0$, the GOS is equal to OOS, our calculated GOS is also in good agreement with experimental OOS values [32,35]. It is interesting to note that our calculated GOS are in closer agreement with recent IXS measurement [15] than previous EELS experiments [11,12], especially around the minima point (higher momentum transfer K). Because the GOS are determined by EELS experiment on the condition that the first Born approximation is satisfied, which strongly depends on the incident electron energies used in the experiments. On the other side, the GOS are measured by IXS experiment directly [15]. The differences between the EELS and IXS results at higher K demonstrate that the first Born approximation is not adequate for describing the electron scattering process at large scattering angles (i.e., large momentum transfer K) at incident energy of 2500 eV.

III. SUMMARY

We would like to conclude with the following comments. Using our modified R-matrix code R-eigen [25], we can directly calculate the short-range scattering matrices with good analytical properties in the entire energy region, from which we can obtain all energy levels and the related scattering cross sections with accuracies comparable to spectroscopic precision. With the corresponding high-quality eigenchannel wave functions, various transition matrix elements can be readily calculated, such as the generalized oscillator strength densities (GOSD). The GOSD is directly related to the high-energy electron impact excitation cross sections. In eigenchannel representation, the GOS matrix elements of the excited states in an eigenchannel form a surface, which is a smooth function of the momentum transfers and the excitation energies. From such smooth GOS matrix elements, we can obtain the GOSD of any specific excited state through multichannel quantum defect theory, e.g., infinite Rydberg (including a strongly perturbed one), autoionization, and continuum states. As an example, we show the calculation results of an Ar atom, which are in good agreement with available benchmark experiments [11,12,15]. The present calculation method of the GOSD from an initial state to final channels can be extended to the case of initial channels to final channels [36], which will be of great importance to astrophysical studies.

ACKNOWLEDGMENTS

This work is supported by the Ministry of Science and Technology and Ministry of Education of China, the Key grant Project of Chinese Ministry of Education (NO.306020), the National Natural Science Foundation of China (Grants No. 11274035, No. 11328401, No. 11275029, 11371218, 11474031, and 11474034) the National High-Tech ICF Committee in China and the Yin-He Super-Computer Center, Institute of Applied Physics and Mathematics, Beijing, China, and National Basic Research Program of China (2011CB921501 and 2013CB922200).

[1] G. Cooper, A. P. Hitchcock, and C. A. Chatzidimitriou-Dreismann, Phys. Rev. Lett. **100**, 043204 (2008); A. P. Hitchcock, J. Electron Spectrosc. Relat. Phenom. **112**, 9 (2000); M. S. Schoffler *et al.*, Science **320**, 920 (2008); M. Foster, J. L. Peacher, M. Schulz, D. H. Madison, Z. Chen, and H. R. J. Walters, Phys. Rev. Lett. **97**, 093202 (2006); P. V. Johnson *et al.*, J. Geophys. Res. **110**, 311 (2005); **A11**, 311 (2005); M. A. Khakoo, P. V. Johnson, I. Ozkay, P. Yan, S. Trajmar, and I. Kanik, Phys. Rev. A **71**, 062703 (2005); G. Katumba *et al.*, Solar Energy Mater. Sol. Cells **92**, 1285 (2008); I. Kuchiwaki *et al.*, *ibid.* **92**, 71 (2008); K. T. Moore and G. van der Laan, Rev. Mod. Phys. **81**, 235 (2009); G. Yang, R. F. Klie, and Q. Ramasse, Phys. Rev. B **78**, 153109 (2008); K. T. Moore, Micron **41**, 336 (2010).

[2] M. Inokuti, Rev. Modern Phys. **43**, 297 (1971).

[3] M. Inokuti, Y. Itikawa, J. E. Turner, Rev. Modern Phys. **50**, 23 (1978).

[4] M. I. Syrkin, Phys. Rev. A **50**, 2284 (1994).

[5] E. Fermi nuovo, Cemento **11**, 157 (1934).

[6] U. Fano, Ann. Rev. Nucl. Sci. **13**, 1 (1963).

[7] A. Akar, H. Gumus, Radiation Physics and Chemistry **73**, 196 (2005).

[8] B. P. Xie, L. F. Zhu, K. Yang, B. Zhou, N. Hiraoka, Y. Q. Cai, Y.Yao, C.Q.Wu, E. L. Wang, and D. L. Feng, Phys. Rev. A **82**, 032501 (2010), and references therein; L. F. Zhu, L. S.Wang, B. P. Xie, K. Yang, N. Hiraoka, Y. Q. Cai, and D. L. Feng, J. Phys. B **44**, 025203 (2011), and references therein; X. J. Liu, L. F. Zhu, Z. S. Yuan, W. B. Li, H. D. Cheng, J. M. Sun, and K. Z. Xu, J. Electron Spectrosc. Relat. Phenom. **135**, 15 (2004).

[9] K. Z. Xu, R. F. Feng, S. L. Wu, Q. Ji, X. J. Zhang, Z. P. Zhong, and Y. Zheng, Phys. Rev. A **53**, 3081 (1996).

[10] H. D. Cheng, L. F. Zhu, Z. S. Yuan, X. J. Liu, J. M. Sun, W. C. Jiang, and K. Z. Xu, Phys. Rev. A **72**, 012715 (2005).

[11] L. F. Zhu, H. D. Cheng, Z. S. Yuan, X. J. Liu, J. M. Sun, and K. Z. Xu, Phys. Rev. A **73**, 042703 (2006).

[12] L. F. Zhu, H. Yuan, W. C. Jiang, F. X. Zhang, Z. S. Yuan, H. D. Cheng, and K. Z. Xu, Phys. Rev. A **75**, 032701 (2007).

[13] W. B. Li, L. F. Zhu, X. J. Liu, Z. S. Yuan, J. M. Sun, H. D. Cheng, Z. P. Zhong, and K. Z. Xu, Phys. Rev. A **67**, 062708 (2003).

[14] L. F. Zhu, W. Q. Xu, K. Yang, Z. Jiang, X. Kang, B. P. Xie, D. L. Feng, N. Hiraoka, and K. D. Tsuei, Phys. Rev. A **85**, 030501 (R) (2012).

[15] X. Kang, K. Yang, Y. W. Liu, W. Q. Xu, N. Hiraoka, K. D. Tsuei, P. F. Zhang, and L. F. Zhu, Phys. Rev. A **86**, 022509 (2012).

[16] H. A. Bethe, Ann. Phys. (Leipzig) **397**, 325 (1930).

[17] K. J. Miller, J. Chem. Phys. **59**, 5639 (1973); I. I. Shimamura, J. Phys. Soc. Jpn. **30**, 824 (1971).

[18] P. S. Ganas and A. E. S. Green, Phys. Rev. A **4**, 182 (1971); T. C. Wong, J. S. Lee, and R. A. Bonham, *ibid.* **11**, 1963 (1975); Y.-K. Kim, M. Inokuti, G. E. Chamberlain, and S. R. Mielczarek, Phys. Rev. Lett. **21**, 1146 (1968).

[19] Z. Chen, A. Z. Msezane, and M. Ya. Amusia, Phys. Rev. A **60**, 5115 (1999); **61**, 030703 (R) (2000); Z. Chen and A. Z. Msezane, J. Phys. B **33**, 2135 (2000); Z. Chen, N. Cherepkov, and A. Z. Msezane, Phys. Rev. A **67**, 024701 (2003).
[20] X. Y. Han and J. M. Li, Phys. Rev. A. **74**, 062711 (2006).
[21] M. J. Seaton, Rep. Prog. Phys. **46**, 167 (1983); J. M. Li, Acta. Phys. Sin. **29**, 419 (1980) (in Chinese).
[22] C. M. Lee and K. T. Lu, Phys. Rev. A. **8**, 1241 (1973).
[23] W. Huang, Y. Zou, X. M. Tong, and J. M. Li, Phys. Rev. A. **52**, 2770 (1995); Y. Zou, X. M. Tong, and J. M. Li, Acta. Phys. Sin. **44**, 50 (1995) (in Chinese).
[24] U. Fano and C. M. Lee, Phys. Rev. Lett. **31**, 1573 (1973); C. M. Lee, Phys. Rev. A. **10**, 584 (1974); U. Fano, J. Opt. Soc. Am. **65**, 979 (1975); M. Aymar, C. H. Greene, and E. Luc-Koenig, Rev. Mod. Phys. **68**, 1015 (1996).
[25] X. Gao and J.-M. Li, Chin. Phys. Lett. **29**, 033101 (2012); Phys. Rev. A **89**, 022710 (2014).
[26] Y. Ralchenko, A. E. Kramida, J. Reader, and NIST ASD Team (2008). NIST Atomic Spectra Database (version 3.1.5) [online]. Available: http://physics.nist.gov/PhysRefData/ASD/levels_form.html [2010, January 7] National Institute of Standards and Technology, Gaithersburg, MD.
[27] U. Fano and J. W. Cooper, Rev. Mod. Phys. **40**, 441 (1968).
[28] P.G. Burke and W. D. Robb, Adv. At. Mol. Phys. **11**, 143 (1975); K. A. Berrington, W. B. Eissner, and P. H. Norrington, Comput. Phys. Commun. **92**, 290 (1995); K. A. Berrington *et al.*, J. Phys. B: At. Mol. Phys. **20**, 6379 (1987).
[29] J. J. Chang, J. Phys. B. **10**, 3335 (1977); P. H. Norrington and I. P. Grant, *ibid.* **20**, 4869 (1987); S. Ait-Tahar, I. P. Grant, and P. H. Norrington, Phys. Rev. A. **54**, 3984 (1996).
[30] J.-M. Li, L. V. Ky, Y.-Z. Qu, J. Yan and P.-H. Zhang, Phys. Rev. A. **55**, 3239 (1997).
[31] X. M. Tong, L. Yang, and J. M. Li, Acta. Phys. Sin. **38**, 407 (1989) (in Chinese).
[32] S. L. Wu, Z. P. Zhong, R. F. Feng, S. L. Xing, B. X. Yang, and K. Z. Xu, Phys. Rev. A **51**, 4494 (1995).
[33] G. P. Li, T. Takayanagi, K. Wakiya, H. Suzuki, T. Ajiro, S. Yagi, S. S. Kano, and H. Takuma, Phys. Rev. A **38**, 1240 (1988).
[34] Q. Ji, S. L. Wu, R. F. Feng, X. J. Zhang, L. F. Zhu, Z. P. Zhong, K. Z. Xu, and Y. Zheng, Phys. Rev. A **54**, 2786 (1996).
[35] W. B. Westerveld, Th. F. A. Mulder, and J. Van Eck, J. Quant. Spectrosc. Radiat. Transfer **21**, 533 (1979).
[36] C. Zhu, J. G. Wang, Y. Z. Qu, and J. M. Li, Phys. Rev. A **57**, 1747 (1998).